

Polarizability and alignment of dielectric nanoparticles in an external electric field: Bowls, dumbbells, and cuboids

Bas W. Kwaadgras,^{1,a)} Maarten Verdult,² Marjolein Dijkstra,¹ and René van Roij²

¹*Soft Condensed Matter, Debye Institute for Nanomaterials Science, Utrecht University, Princetonplein 5, 3584 CC Utrecht, the Netherlands*

²*Institute for Theoretical Physics, Utrecht University, Leuvenlaan 4, 3584 CE Utrecht, the Netherlands*

(Received 18 May 2011; accepted 19 August 2011; published online 3 October 2011)

We employ the coupled dipole method to calculate the polarizability tensor of various anisotropic dielectric clusters of polarizable atoms, such as cuboid-, bowl-, and dumbbell-shaped nanoparticles. Starting from a Hamiltonian of a many-atom system, we investigate how this tensor depends on the size and shape of the cluster. We use the polarizability tensor to calculate the energy difference associated with turning a nanocluster from its least to its most favorable orientation in a homogeneous static electric field, and we determine the cluster dimension for which this energy difference exceeds the thermal energy such that particle alignment by the field is possible. Finally, we study in detail the (local) polarizability of a cubic-shaped cluster and present results indicating that, when retardation is ignored, a bulk polarizability cannot be reached by scaling up the system. © 2011 American Institute of Physics. [doi:10.1063/1.3637046]

I. INTRODUCTION

Monodisperse (colloidal) particles with a wide variety of shapes can nowadays be synthesized in the nanometer to micrometer size regime.^{1,2} These particles can serve as building blocks for new materials and devices with great technological potential. Self-assembly of the particles is an important process by which large-scale nano-structures can be formed. This self-assembly process can be spontaneous in the case of favorable thermodynamic conditions and suitable effective particle-particle interactions,^{3–10} but can also be steered and further manipulated by external fields. Rodlike particles in a liquid dispersion, for instance, can spontaneously align at sufficiently high concentrations solely due to their excluded volume interactions,¹¹ but their self-organization has also been driven by external magnetic or electric fields,^{12–16} by substrates that preferentially orient the rods,^{17,18} or by fluid flow.¹⁹ Also, more complicated shapes have been synthesized and studied, for instance, dumbbells,^{2,20–22} cubes,²³ and bowls.^{21,24,25}

In this article we study the electric-field assisted alignment of anisotropic nanoparticles by calculating their polarizability tensor starting from a microscopic picture of polarizable units that we call “united atoms” or just briefly “atoms,” even though also larger units could have been taken. We only consider dielectric particles,^{26,27} and not metallic particles.^{28–30} From the polarizability tensor of a non-spherical cluster of atoms, the orientation-dependent electrostatic energy follows, and hence the cluster’s ability to align in an external electric field. We focus here on cuboid-shaped (rods and platelets), bowl-shaped, and dumbbell-shaped particles, for which we consider various shape and size parameters. The polarizability of similar shapes have in recent years

been under study using continuum theory^{31–35} and on several occasions we briefly compare those results to ours.

Our calculations are based on the coupled dipole method (CDM), a formalism introduced by Renne and Nijboer in the 1960s.^{36,37} In the CDM, each atom in a cluster is treated as a Lorentz atom (or Drude oscillator), in which the electron is bound to the nucleus by a harmonic force. The atoms have no permanent electric dipole moment, but their dipole moments are induced by the local electric field. This model has been shown to yield the van der Waals interaction between two atoms.^{36,38,39} In the CDM, many such dipolar atoms interact and the potential energy, including all many-body effects, can be calculated from the eigenfrequencies of a set of coupled harmonic oscillators, yielding forces equivalent to Lifschitz’s quantum-electrodynamic fluctuation theory.⁴⁰ Due to its full many-body nature the CDM is more accurate than continuum theories based on pairwise summations of atomic van der Waals interactions, as employed in, e.g., the Hamaker-de Boer approach^{41,42} that underlies the treatment of dispersion forces in DLVO-theory.^{43,44} In this article we do not consider solvent effects explicitly.

II. FORMALISM OF THE CDM: POTENTIAL ENERGY, POLARIZABILITY, AND ORIENTATIONAL ENERGY

A. Introduction

In the Lorentz model for atoms in an external electric field, an atom is modeled as a dipole consisting of a nucleus and an electron bound to it by a harmonic force. Thus, if the electron is at a nonzero distance from the nucleus, the atom is effectively an induced electric dipole. In this simple model, the displacement \mathbf{u} of the electron with respect to the nucleus, and thus the atom’s polarization $\mathbf{p} = e\mathbf{u}$, is linearly dependent

^{a)} Author to whom correspondence should be addressed. Electronic mail: b.w.kwaadgras@uu.nl.

on the local electric field \mathbf{E} that the atom is subjected to,

$$e\mathbf{u} = \mathbf{p} = \alpha_0\mathbf{E},$$

where e is the elementary charge. Here, α_0 is the polarizability of the atom, given by

$$\alpha_0 = \frac{e^2}{m_e\omega_0^2}, \quad (1)$$

where m_e denotes the electron mass and ω_0 is the angular frequency associated with the harmonic force that binds the electron to the nucleus.⁴⁵ Since an electric dipole will produce a nonzero electric field in its surroundings, two of these Lorentz atoms will interact, mediated by the electric field. It has been shown that this dipole-dipole interaction yields the unretarded Van der Waals interaction ($\propto r^{-6}$) between the pair of atoms (at large separation r).³⁶ If N of these atoms are brought together and allowed to interact, the dipole-dipole interactions will influence the electric properties of the cluster as a whole. In general, the total polarizability of the cluster cannot be expected to equal $N\alpha_0$, but will instead be modified because the atoms are subject to each other's induced electric field.

B. Static polarizability and orientational energy of dipole clusters in an external electric field

The Hamiltonian of a set of N Lorentz atoms at fixed positions \mathbf{r}_i ($i = 1, \dots, N$) has been given and studied in Refs. 27, 36, 38, 46–48. In the present work, we use the same Hamiltonian, but add an extra term to allow for an externally exerted, spatially homogeneous, electric field \mathbf{E}_0 , such that the complete expression for the Hamiltonian is

$$H = \sum_{i=1}^N \frac{\mathbf{k}_i^2}{2m_e} + \sum_{i=1}^N \frac{m_e\omega_0^2\mathbf{u}_i^2}{2} - \sum_{i,j=1}^N \frac{e^2\mathbf{u}_i \cdot \mathbf{T}_{ij} \cdot \mathbf{u}_j}{2} - \sum_{i=1}^N e\mathbf{u}_i \cdot \mathbf{E}_0, \quad (2)$$

where we denote the momentum of the electron of atom i by \mathbf{k}_i . The 3×3 matrix \mathbf{T}_{ij} is the dipolar tensor, given in terms of the separation vector $\mathbf{r}_{ij} = \mathbf{r}_i - \mathbf{r}_j$ of atoms i and j , by

$$\mathbf{T}_{ij} = \begin{cases} \frac{(3\mathbf{r}_{ij}\mathbf{r}_{ij}/|\mathbf{r}_{ij}|^2 - \mathbf{I})}{|\mathbf{r}_{ij}|^3}, & \text{if } i \neq j, \\ \mathbf{0}, & \text{if } i = j \end{cases},$$

where \mathbf{I} denotes the 3×3 identity matrix and $\mathbf{0}$ denotes the 3×3 null matrix. Note that the dipolar tensor is not only symmetric in its indices, $\mathbf{T}_{ij} = \mathbf{T}_{ji}$, but also symmetric in its elements, $\mathbf{T}_{ij} = \mathbf{T}_{ij}^T$. As is clear from the Hamiltonian equation (2) and the form of \mathbf{T}_{ij} , this model describes interatomic interactions in an instantaneous, nonretarded way. Therefore, the validity of the theory is limited to model systems where the relevant length scales are small enough for the speed of light to be essentially infinite.

We now introduce $3N$ -dimensional vectors \mathcal{K} , \mathcal{U} , and \mathcal{E}_0 , which are built up from the \mathbf{k}_i , \mathbf{u}_i , and N copies of \mathbf{E}_0 , res-

spectively. We also introduce a $3N \times 3N$ -dimensional matrix \mathcal{T} , built up from the \mathbf{T}_{ij} . In terms of these objects, the Hamiltonian equation (2) is given by

$$H = \frac{\mathcal{K}^2}{2m_e} + \frac{1}{2}m_e\omega_0^2\mathcal{U} \cdot (\mathcal{I} - \alpha_0\mathcal{T}) \cdot \mathcal{U} - e\mathcal{U} \cdot \mathcal{E}_0,$$

where α_0 is given in Eq. (1), and \mathcal{I} denotes the $3N \times 3N$ -dimensional identity matrix. Next, we introduce a $3N$ -dimensional vector \mathcal{U}_0 that satisfies

$$m_e\omega_0^2(\mathcal{I} - \alpha_0\mathcal{T}) \cdot \mathcal{U}_0 = e\mathcal{E}_0, \quad (3)$$

and use it to complete the square in the Hamiltonian, obtaining

$$H = H_0 + V_E \quad (4)$$

with

$$H_0 = \frac{\mathcal{K}^2}{2m_e} + \frac{1}{2}m_e\omega_0^2(\mathcal{U} - \mathcal{U}_0) \cdot (\mathcal{I} - \alpha_0\mathcal{T}) \cdot (\mathcal{U} - \mathcal{U}_0), \quad (5)$$

$$V_E = -\frac{1}{2}\alpha_0\mathcal{E}_0 \cdot (\mathcal{I} - \alpha_0\mathcal{T})^{-1} \cdot \mathcal{E}_0. \quad (6)$$

Note that V_E is constant with respect to the generalized momenta and coordinates \mathcal{K} and $\mathcal{U} - \mathcal{U}_0$, respectively. The $3N$ oscillatory modes associated with the (harmonic) Hamiltonian H_0 are given by

$$(\mathcal{U}^{(k)} - \mathcal{U}_0)(t) = (\mathcal{U}^{(k)} - \mathcal{U}_0)(0) \exp(-i\omega_k t), \quad (k = 1, \dots, 3N), \quad (7)$$

where the amplitude vectors $(\mathcal{U}^{(k)} - \mathcal{U}_0)(0)$ and the frequencies ω_k are given by an eigenvalue equation for the matrix $(\mathcal{I} - \alpha_0\mathcal{T})$:

$$\frac{\omega_k^2}{\omega_0^2}(\mathcal{U}^{(k)} - \mathcal{U}_0)(0) = (\mathcal{I} - \alpha_0\mathcal{T})(\mathcal{U}^{(k)} - \mathcal{U}_0)(0). \quad (8)$$

If we denote the eigenvalues of the matrix \mathcal{T} by λ_k , it is seen that the eigenvalues of $(\mathcal{I} - \alpha_0\mathcal{T})$ are $(1 - \alpha_0\lambda_k)$, and thus that the allowed frequencies are

$$\omega_k = \omega_0\sqrt{1 - \alpha_0\lambda_k}.$$

Assuming the system to be in the electronic ground state, we arrive at the total potential energy

$$V = V_0 + V_E, \quad (9)$$

where V_0 is the ground state energy of H_0 , given by the sum of mode frequencies,

$$V_0 = \frac{1}{2}\hbar \sum_{k=1}^{3N} \omega_k, \quad (10)$$

where \hbar is the reduced Planck constant.

We note that V_0 depends solely on the matrix $(\mathcal{I} - \alpha_0\mathcal{T})$ and, thus, only on the relative coordinates \mathbf{r}_{ij} of the atoms with respect to each other. It follows that this term is completely independent of the orientation of the cluster with respect to the electric field. In the absence of other clusters, V_0 can therefore be interpreted as the self-energy of the cluster;

in the presence of other clusters, the term also contains the interaction energy between the clusters.⁴⁶ For the analysis of the response of the clusters to an external electric field, however, we turn to the second term V_E of Eq. (9): this term, given in Eq. (6), contains all the orientational potential energy of the cluster in the external electric field.

Clearly, the Hamiltonian of Eq. (4) describes a set of harmonic oscillators with equilibrium positions given by \mathcal{U}_0 and a shifted ground state energy V . Using this interpretation of \mathcal{U}_0 , we show, in the following, that V_E is the energy of the total time-averaged dipole moment of the cluster in the external electric field. We first rewrite Eq. (3) in terms of the mean polarization vector $\mathcal{P} \equiv e\mathcal{U}_0$,

$$(\mathcal{I} - \alpha_0\mathcal{T}) \cdot \mathcal{P} = \alpha_0\mathcal{E}_0, \quad (11)$$

and use this equation, in combination with the expression for V_E given in Eq. (6), to derive

$$V_E = -\frac{1}{2}\mathcal{E}_0 \cdot \mathcal{P} = -\frac{1}{2}\mathbf{E}_0 \cdot \mathbf{p}_c, \quad (12)$$

where

$$\mathbf{p}_c \equiv \sum_{i=1}^N \mathbf{p}_i \quad (13)$$

denotes the total polarization of the cluster and $\mathbf{p}_i \equiv e\mathbf{u}_{0,i}$ denotes the mean (time-averaged) polarization of atom i , as given by the elements of \mathcal{P} . From the form of Eq. (12), it is clear that V_E is the energy of an induced dipole \mathbf{p}_c in an electric field \mathbf{E}_0 .⁴⁵ If we divide the matrix $(\mathcal{I} - \alpha_0\mathcal{T})^{-1}$ into 3×3 sub-blocks \mathbf{D}_{ij} , it can easily be seen from Eq. (11) that $\mathbf{p}_i = \alpha_0 \sum_j \mathbf{D}_{ij} \cdot \mathbf{E}_0$, and thus that

$$\mathbf{p}_c = \alpha_0 \sum_{i,j=1}^N \mathbf{D}_{ij} \cdot \mathbf{E}_0 \equiv \boldsymbol{\alpha}_c \cdot \mathbf{E}_0, \quad (14)$$

where we define the 3×3 cluster polarizability matrix by

$$\boldsymbol{\alpha}_c \equiv \alpha_0 \sum_{i,j=1}^N \mathbf{D}_{ij}. \quad (15)$$

An alternative derivation of Eqs. (11)–(14) is given in Ref. 26. Note that $\boldsymbol{\alpha}_c$ depends solely on the spatial configurational properties of the cluster, not on the external electric field. Moreover, one can prove mathematically that $\boldsymbol{\alpha}_c$ is a symmetric matrix, as long as each atom has an equal polarizability α_0 .⁴⁹ This symmetry of $\boldsymbol{\alpha}_c$ implies that its eigenvectors are orthogonal, which in turn implies that it is always possible to transform the system to an orthogonal basis, spanned by these eigenvectors, in which $\boldsymbol{\alpha}_c$ is diagonal.

Computationally, Eq. (15) is not a practical way of determining $\boldsymbol{\alpha}_c$, since it involves the very expensive operation of explicitly calculating the inverse of a large matrix. Numerically, the most favorable approach is to use Eq. (14): after choosing a suitable coordinate system, we apply an electric field in the x direction and calculate the cluster polarization by solving Eq. (11). Efficient numerical algorithms for solving a set of linear equations are readily available, for example, in the LAPACK package.⁵⁰ Having solved Eq. (11) for \mathcal{P} , we calculate the sum in Eq. (13), then divide the resulting vector

by the electric field strength; the result is the first column of $\boldsymbol{\alpha}_c$. To gain the remaining two columns, this procedure is then repeated in the other two Cartesian directions.

If we were to neglect the dipolar interactions within the cluster, its polarization would be simply $N\alpha_0\mathbf{E}_0$, i.e., the cluster polarizability would simply be a scalar $N\alpha_0$. The ratio of the “actual” polarizability $\boldsymbol{\alpha}_c$ and this “naive” guess for the polarizability,

$$\mathbf{f} = \frac{\boldsymbol{\alpha}_c}{N\alpha_0}, \quad (16)$$

is a measure of how much the polarizability is enhanced due to dipole-dipole interactions and may therefore be called the “enhancement factor” of the dipole cluster.²⁶

In terms of $\boldsymbol{\alpha}_c$, we can rewrite Eq. (12) compactly as

$$V_E = -\frac{1}{2}\mathbf{E}_0 \cdot \boldsymbol{\alpha}_c \cdot \mathbf{E}_0. \quad (17)$$

This expression can then be written in terms of the eigenvalues α_n and the corresponding normalized eigenvectors \mathbf{v}_n ($n = 1, 2, 3$) of $\boldsymbol{\alpha}_c$:

$$\begin{aligned} V_E &= -\frac{1}{2} \sum_{n,m=1}^3 (\mathbf{E}_0 \cdot \mathbf{v}_n)(\mathbf{v}_n \cdot \boldsymbol{\alpha}_c \cdot \mathbf{v}_m)(\mathbf{v}_m \cdot \mathbf{E}_0) \\ &= -\frac{1}{2} \sum_{n=1}^3 (\mathbf{E}_0 \cdot \mathbf{v}_n)^2 \alpha_n. \end{aligned} \quad (18)$$

In the first line, we inserted twice a complete orthonormal set of eigenvectors, while, in the second line, we made use of the fact that $\boldsymbol{\alpha}_c \cdot \mathbf{v}_m = \alpha_m \mathbf{v}_m$ and $\mathbf{v}_n \cdot \mathbf{v}_m = \delta_{nm}$. The inner products obey the rule $\sum_n (\mathbf{E}_0 \cdot \mathbf{v}_n)^2 = E_0^2$, from which it follows that $\sum_{n=1}^3 (\mathbf{E}_0 \cdot \mathbf{v}_n)^2 \alpha_n \leq \alpha_{max} E_0^2$, where $\alpha_{max} = \max(\{\alpha_n\})$ and the equality is achieved if and only if $\mathbf{E}_0 \parallel \mathbf{v}_{max}$, where \mathbf{v}_{max} is the eigenvector corresponding to α_{max} . It follows that V_E is minimized by an electric field in the direction of \mathbf{v}_{max} . A similar reasoning leads to the observation that V_E is maximized by an electric field in the direction of the eigenvector with the smallest eigenvalue, α_{min} . The difference $|\Delta|$ between maximum and minimum orientational energy V_E is thus given by

$$|\Delta| = \frac{1}{2} (\alpha_{max} - \alpha_{min}) E_0^2.$$

Here, for later purposes, we intentionally kept the freedom of choosing the sign of Δ .

C. Rotationally symmetric clusters

The bowl- and dumbbell-shaped nanoparticles considered in this article are clusters with an axis of rotational symmetry. The rotational invariance implies that the polarization that would be induced by an electric field in the direction of the symmetry axis must lie along this symmetry axis, and therefore that this axis is an eigenvector of the cluster’s polarizability matrix $\boldsymbol{\alpha}_c$. Since it is known that $\boldsymbol{\alpha}_c$ must be a symmetric matrix, we know that its eigenvectors must be perpendicular to each other. This leads to the conclusion that the preferred direction of any rotationally symmetric cluster must either lie along the rotational symmetry axis or perpendicular

to it. In this article, we always choose our coordinate system such that this rotational symmetry axis lies along the z axis, and choose the x and y directions such that α_c is diagonal (i.e., the Cartesian axes are the eigenvectors of α_c). Moreover, for rotationally symmetric clusters, $\alpha_{xx} = \alpha_{yy}$, and hence we are left with only two independent entries on the diagonal of α_c , one of which will be α_{max} and the other will be α_{min} . For the remainder of this article, we now define the orientational energy difference as⁵¹

$$\Delta \equiv \frac{1}{2}(\alpha_{zz} - \alpha_{xx})E_0^2, \quad (19)$$

where we choose the sign of Δ such that Δ is positive when the preferred direction of the cluster is along the rotational symmetry axis (which is equivalent to $\alpha_{zz} > \alpha_{xx}$).

Using Eq. (16), we can write Eq. (19) as

$$\Delta = \frac{1}{2}\Delta_f N \alpha_0 E_0^2, \quad (20)$$

where

$$\Delta_f = f_{zz} - f_{xx}.$$

As will be shown for all the cluster shapes in this article, the quantity Δ_f is largely independent of the cluster size, provided the number of atoms is large enough. In this regime, Δ_f depends only on the shape of the cluster and on the dimensionless interatomic distance $a/\alpha_0^{1/3}$. This assertion does not state anything about the individual values of f_{zz} and f_{xx} as a function of cluster size. From the numerical data, it turns out that these quantities can still depend on cluster size, albeit usually only weakly.

It is of interest to compare Δ to the thermal energy $k_B T$, since only if $\Delta \gtrsim k_B T$, an electric field can be used to orient the particle. Equating $\Delta = k_B T$ we derive the required number of atoms N^* from Eq. (20),

$$N^* = \frac{2k_B T}{\Delta_f \alpha_0 E_0^2}. \quad (21)$$

In Sec. IV, we will use this expression to calculate N^* for bowls and dumbbells and hence estimate the spatial dimensions required for aligning these particles using an electric field.

D. Fourfold rotationally symmetric clusters

One of the discussed cluster shapes in this article is a cluster with a cubic shape. If we choose the coordinate axes along the ribs of the cube, it can be easily seen from symmetry considerations that an electric field applied in the x direction must induce a total cluster polarization $\mathbf{p}_c^{(\text{cube})}$ with a nonzero component only in the x direction. Similarly, the polarizations as a result of electric fields in the y and z directions will also point along the y and z axes, respectively. Because these resulting polarizations are proportional to the columns of $\alpha_c^{(\text{cube})}$, it follows that $\alpha_c^{(\text{cube})}$ must be diagonal in this basis. Moreover, because the cube is invariant under 90° rotations, we do not expect the induced polarization of the cube to be dependent on whether the electric field is applied in the x , y , or z direction and, therefore, the entries on the diagonal of

$\alpha_c^{(\text{cube})}$ must be equal. Hence,

$$\alpha_c^{(\text{cube})} \propto \mathbf{I}. \quad (22)$$

Note that, in this case, both the polarizability and the enhancement factor can be described by a scalar: the former by the proportionality factor between $\alpha_c^{(\text{cube})}$ and \mathbf{I} , the latter by this ‘‘scalar polarizability’’ divided by $N\alpha_0$. Since in this case $\alpha_{xx} = \alpha_{yy} = \alpha_{zz}$, we find, from Eq. (19), that $\Delta = 0$. This kind of cluster will therefore *not* have a preferred orientation within an external electric field. Physically, this is a surprising result since, *a priori*, one could expect an anisotropic cluster such as a cube to prefer to align one of its features (such as its ribs, faces, or vertices) along the electric field. However, simple symmetry arguments negate this expectation. For cuboid-shaped rods and platelets, on the other hand, as is the case for bowls and dumbbells, $\alpha_{xx} = \alpha_{yy} \neq \alpha_{zz}$ and hence $\Delta \neq 0$. In Sec. III, we will use Eq. (21) to calculate N^* for rods and platelets and estimate the minimum size of the particles to align them in an electric field.

E. Units of distance

Throughout the remainder of this paper, we will usually measure lattice spacings in units of $\alpha_0^{1/3}$. The reason is that, throughout the theory, the matrix \mathcal{T} is always multiplied by a factor α_0 . Upon applying this multiplication to the submatrices \mathbf{T}_{ij} , we get

$$\alpha_0 \mathbf{T}_{ij} = \frac{(3\mathbf{s}_{ij}\mathbf{s}_{ij}/|\mathbf{s}_{ij}|^2 - \mathbf{I})}{|\mathbf{s}_{ij}|^3} \quad (i \neq j),$$

where

$$\mathbf{s}_{ij} = \mathbf{r}_{ij}/\alpha_0^{1/3}.$$

Clearly, the relevant parameters are not the \mathbf{r}_{ij} themselves, but rather the dimensionless combinations $\mathbf{s}_{ij} = \mathbf{r}_{ij}/\alpha_0^{1/3}$. Using these dimensionless distances, we thus eliminate the atomic polarizability as an explicit input parameter. At the same time, the dimensionless combinations are $\mathcal{O}(1)$ in magnitude (for typical lattices and atomic polarizabilities), which is convenient for computational purposes. We use the numerical data provided in Ref. 26 to calculate the dimensionless lattice spacing

$$\tilde{a} \equiv a/\alpha_0^{1/3}$$

for several substances, the result of which is listed in Table I. For clarity, we note here that all other physical quantities remain unscaled in this paper.

TABLE I. Lattice spacings a , atomic polarizabilities α_0 , and dimensionless lattice spacings $\tilde{a} \equiv a/\alpha_0^{1/3}$ of some typical substances. (See Ref. 26.)

Substance	$a(\text{\AA})$	$\alpha_0(\text{\AA}^3)$	\tilde{a}
Hexane	6.009	11.85	2.64
Silica	3.569	5.25	2.05
Sapphire	3.486	7.88	1.75

III. DIELECTRIC RODS AND PLATELETS

A simple (but useful) example illustrating the introduced quantities are dielectric rods and platelets. We consider cuboid-shaped clusters, with the atoms on a simple cubic (sc) lattice with a dimensionless lattice constant $\tilde{a} = 2$. Let L be the number of atoms along the edge parallel to the axis of 90° rotational symmetry and l be the number of atoms along the other two edges. Then the shape of the $l \times l \times L$ cuboid is defined by the ratio l/L . This cluster shape is rod-like for $l/L < 1$, cubic-shaped for $l/L = 1$, and platelet-shaped for $l/L > 1$.

The edge of length L of the cuboid is the axis of fourfold rotational symmetry, and we choose the z axis along this edge. In this coordinate system, the polarizability matrix is diagonal with only two independent elements, $\alpha_{xx} = \alpha_{yy}$ and α_{zz} .

A well-known property of dipoles is that it is energetically favorable for them to lie head-to-toe and unfavorable to lie side-by-side. Therefore, for $l/L < 1$ (rods), if we apply an electric field in the z direction, thus inducing a polarization of the dipoles along the “head-to-toe direction,” we expect the dipole-dipole interactions between the atoms to enhance the induced polarization, because there are more dipoles lying head-to-toe than side-by-side. On the other hand, an electric field in the transverse direction (x - y plane) would induce more atomic polarizations lying side-by-side than head-to-toe and therefore, in this case, we expect the interactions to reduce the induced polarization. Also, we expect this effect to be stronger for smaller l/L ratios, since the smaller this ratio, the more extreme the difference in the number of head-to-toe and side-by-side interactions will be. We expect the opposite to happen for $l/L > 1$ (platelets), for similar reasons.

In Fig. 1(a), we plot the elements of the enhancement factor $f_{xx} = \alpha_{xx}/N\alpha_0$ and $f_{zz} = \alpha_{zz}/N\alpha_0$, as a function of l/L , for $L = 10$. Our heuristic expectation that the enhancement in the z direction is larger than that in the x direction for $l/L < 1$ is confirmed by this plot. For small l/L , the interatomic interactions reduce the polarization when the electric field is applied in the x direction, while they enhance it when it is applied in the z direction. However, f_{xx} becomes larger than unity for $l/L \gtrsim 0.73$, where atomic interactions enhance the polarization in both directions. We note that f_{xx} and f_{zz} cross over at $l/L = 1$, which is the special case of a dielectric cube-shaped particle. Here, the enhancements in both directions equal each other, as was predicted in Eq. (22). The value of the enhancements for $l/L = 1$ is $f_{xx} = f_{zz} \approx 1.05687$. The L -dependence of the enhancement factor of cubic clusters will be discussed in Sec. V. For $l/L > 1$ (platelets), the cuboid polarizability is more enhanced in the x direction than in the z direction, and f_{zz} becomes smaller than unity for $l/L \gtrsim 1.17$, which means that the interatomic interactions start reducing the z -polarizability for sufficiently flat platelets.

In Fig. 1(b), we plot the orientational energy difference Δ [as defined in Eq. (19)], for a typical electric field strength of $E_0 = 100 \text{ V mm}^{-1}$, an atomic polarizability $\alpha_0 = 5.25 \text{ \AA}^3$, at room temperature ($T = 293 \text{ K}$), as a function of the number of cluster atoms, for several values of $l/L < 1$ (rods). The lattice is simple cubic with lattice spacing $a = 2\alpha_0^{1/3} \approx 3.48 \text{ \AA}$. Clearly, Δ is linear in the number of particles. We fit the

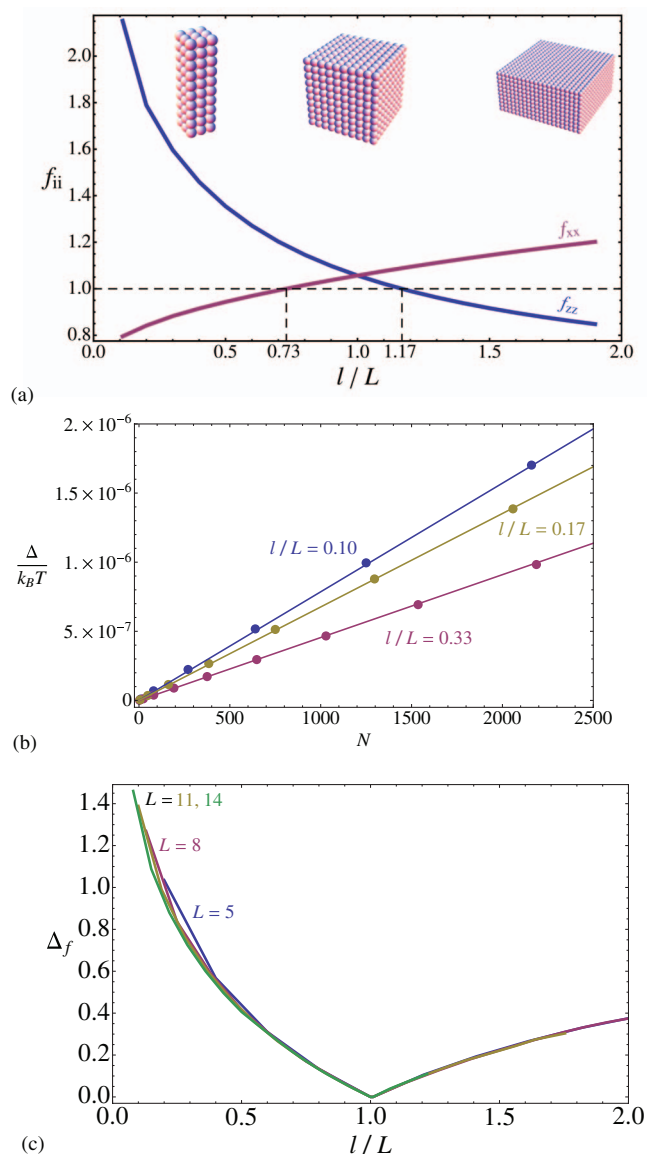


FIG. 1. Properties of an $l \times l \times L$ cuboid-shaped cluster of atoms with atomic polarizability α_0 on a simple cubic lattice with spacing $\tilde{a} = 2$. (a) The elements f_{xx} (red) and f_{zz} (blue) of the enhancement factor matrix as a function of the shape parameter l/L , for $L = 10$. Note that $f_{xx} = 1$ at $l/L \approx 0.73$, $f_{zz} = 1$ at $l/L \approx 1.17$, and $f_{xx} = f_{zz} = 1.05687$ at $l/L = 1$. (b) The difference $\Delta_f = f_{zz} - f_{xx}$ of the enhancement factor elements as a function of l/L , for several values of L . (c) The energy difference Δ (in units of $k_B T$) of turning the cuboidal rod from its least to its most favorable orientation in an external electric field, as a function of the number of atoms N in a rod, with shape parameters $l/L = 0.10$, $1/6 \approx 0.17$, and $1/3 \approx 0.33$. System parameters are given in the text, and the solid lines are linear fits to the data.

data to the functional form of Eq. (20), with Δ_f being fit parameter.

For sufficiently large N , we can confirm from Fig. 1(b) that Δ_f is constant with respect to the particle size, and that hence Δ_f depends only on the shape parameter l/L (save for the internal parameter \tilde{a}). As mentioned before, the individual values for f_{zz} and f_{xx} are allowed to vary with size, but the numerical data shows that they do so only slightly in the case of rods.

As an example, for $l/L = 0.10$, we find, for the parameters of Fig. 1(b), that $\Delta_f \approx 1.1$. By substituting the aforementioned numerical data into Eq. (21), it follows that $N^* \approx 1.3 \times 10^9$. Using the shape parameter $l/L = 0.1$, the number of atoms along the long edge of the cuboid is calculated as $L^* = (100N^*)^{1/3} \approx 5.0 \times 10^3$ which, using $a \approx 3.48 \text{ \AA}$, corresponds to a physical length of the long edge of $\sim 1.8 \mu\text{m}$ and corresponding length of the short edges of $0.18 \mu\text{m}$.

A simple order-of-magnitude calculation shows that retardation effects, which are not included in our theory, become important when length scales are of the order of $\sim 500 \text{ nm}$. The estimate of $1.8 \mu\text{m}$ for alignment exceeds this length scale and thus, retardation effects are expected to be important. The exact magnitude of the error this produces in our estimate is hard to determine without including retardation effects in the CDM, but the expectation is that the error will be marginal, since our estimated length scale does not dramatically exceed the 500 nm boundary.

In Fig. 1(c), we plot Δ_f as a function of l/L , for several values of L . Interestingly, these graphs overlap for sufficiently large N , again confirming the independence of Δ_f of L . It appears that for cuboids, a ‘‘sufficiently large N ’’ is easily achieved: already for $l \times l \times 5$ cuboids, there is almost perfect collapse of the data.

A. Dielectric strings

A special case of a dielectric rod is a cluster consisting of L Lorentz atoms positioned on a straight line, separated by an interatomic distance a . This shape can be viewed as a $L \times 1 \times 1$ cuboid for which l/L becomes arbitrarily small as L increases. We will briefly discuss this cluster shape here, because it has been investigated previously.²⁶

For lattice spacing $\tilde{a} = 2$, the enhancement factor matrix elements f_{xx} and f_{zz} are plotted, as a function of L in Fig. 2(a). We note that this is not a new result, Kim *et al.* produced a similar plot in Ref. 26. From $f_{zz} > f_{xx}$, it is clear that an electric field applied in the z direction will induce a higher polarization than the one applied in the x direction. The enhancement in the z direction, f_{zz} , is greater than unity, meaning that the interactions enhance the induced polarization, as expected. On the other hand, f_{xx} is smaller than unity, meaning that the polarizability is reduced by the interactions. The limiting value of f_{zz} for $L \rightarrow \infty$ is $f_{zz}(L \rightarrow \infty) \approx 2.5064$ while, in the transverse direction, $f_{xx}(L \rightarrow \infty) \approx 0.7689$.²⁶

In Fig. 2(b), we plot the orientational energy difference equation (19) for three values of the dimensionless interatomic distance \tilde{a} , for a typical electric field strength of $E_0 = 100 \text{ V mm}^{-1}$, an atomic polarizability of 5.25 \AA^3 , and at room temperature ($T = 293 \text{ K}$). To the numerical results, linear functions of the form

$$\Delta = \frac{1}{2} \Delta_f \alpha_0 E_0^2 (L - L_0) \quad (23)$$

have been fitted with Δ_f and L_0 as fit parameters. We note here that Eq. (23) is compatible with Eq. (20) when $L \gg L_0$. In this regime, atomic strings will have a negligible end effect. We usually find that $L_0 \lesssim \mathcal{O}(10)$ so, often, $L \gg L_0$. As an

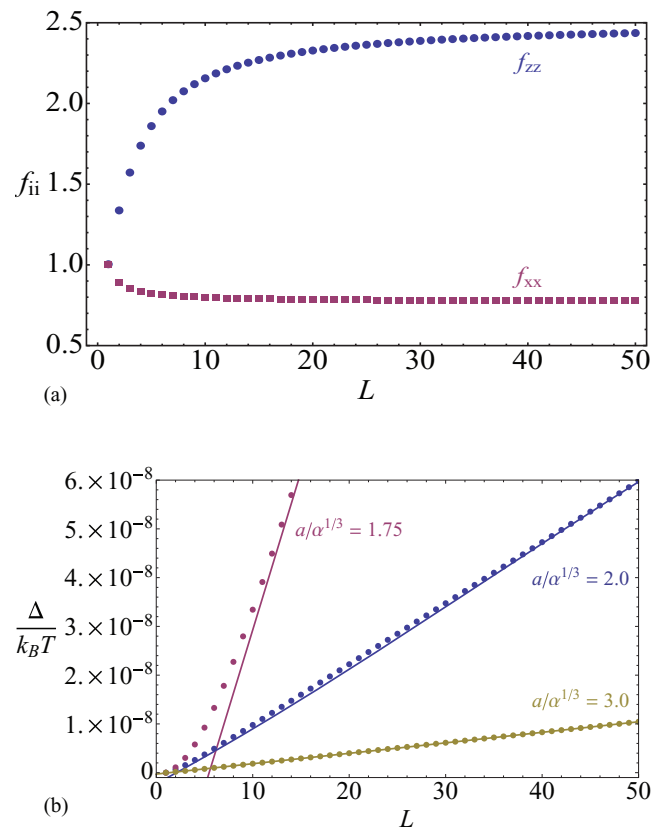


FIG. 2. (a) The diagonal elements f_{xx} (red squares) and f_{zz} (blue circles) of the enhancement factor matrix of a straight line of L dipoles along the z axis. The spacing between the atoms is $\tilde{a} = 2$ (note that for f_{ii} , no other parameters are needed to define this system). (b) The energy difference Δ associated with turning this string from its least to its most favorable orientation in an external electric field $E_0 = 100 \text{ V mm}^{-1}$, for three different values of the dimensionless interatomic distance, $\tilde{a} = 1.75$ (red), $\tilde{a} = 2$ (blue), and $\tilde{a} = 3$ (yellow). Choosing atomic polarizability $\alpha_0^{1/3} = 5.25 \text{ \AA}^3$ (silica), these values correspond to spacings of, respectively, $a \approx 3.04 \text{ \AA}$, 3.48 \AA , and 5.21 \AA . The temperature is $T = 293 \text{ K}$ (room temperature).

example, the fit parameters for $\tilde{a} = 2$ turn out to be

$$\Delta_f \approx 1.72, \quad L_0 \approx 1.98. \quad (24)$$

Using Eqs. (23) and (24), we can make a prediction for the length L^* of an atomic string for which the orientational energy difference becomes of the order of $k_B T$. Equating $\Delta = k_B T$, it is easily seen that

$$L^* = \frac{2k_B T}{\Delta_f \alpha_0 E_0^2} + L_0 \approx 8.1 \times 10^8.$$

Since in this case $a = 2\alpha_0^{1/3} \approx 3.5 \text{ \AA}$, we find a minimum string length of about a meter in order to experience any significant effect from the electric field, which is clearly unphysical.

IV. DIELECTRIC BOWLS AND DUMB BELLS

In this section we consider two other shapes of dipole clusters, namely, bowl-shaped and dumbbell-shaped clusters. As mentioned in Sec. I, these shapes have recently been synthesized and show self-assembly behavior that can be

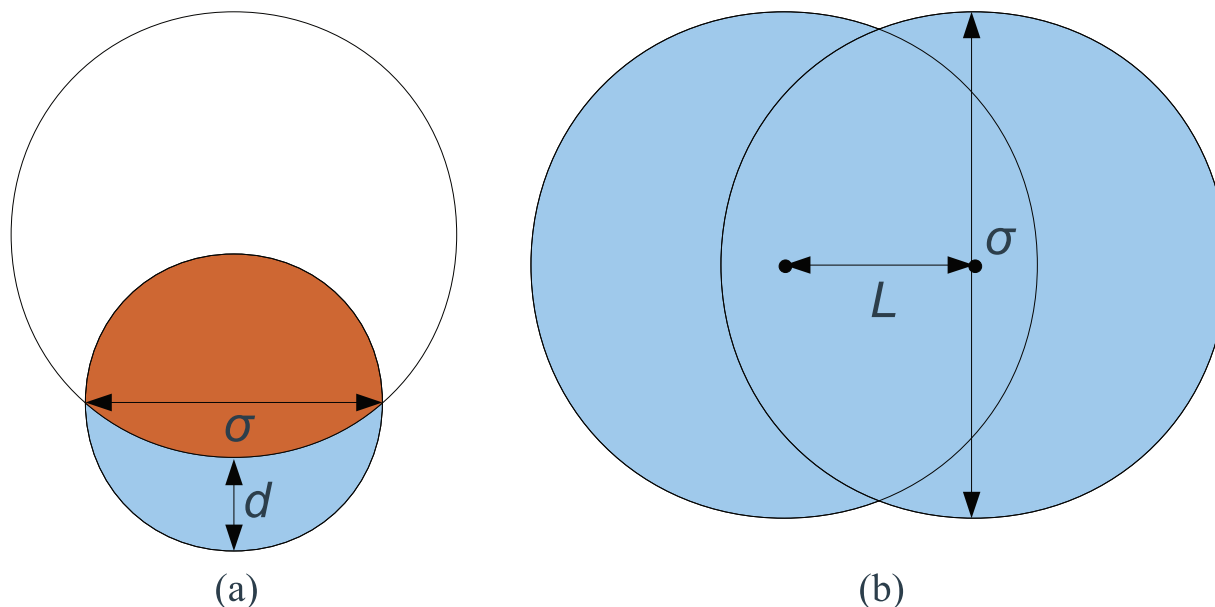


FIG. 3. Construction and definition of parameters for (a) bowl and (b) dumbbell. (a) The bowl diameter σ and the bowl thickness d completely define its shape, as follows. If $d < \sigma/2$, the shape of the bowl is defined by subtracting one sphere from another (the blue area). (See Ref. 21.) If $d > \sigma/2$, we let $d \rightarrow \sigma - d$ and use the same construction, but take the intersection of the spheres instead of the difference (the orange area). Note that in the latter case, the shape is no longer a “bowl” in the traditional sense of the word. (b) The shape of the dumbbell is constructed by adding two (overlapping) spheres. The sphere diameter σ and the distance between the sphere centers L completely define the shape of the dumbbell. Note that if $L > \sigma$, the “dumbbell,” in fact, consists of two separate spheres.

influenced by an external electric field. It is of interest to investigate how the shape and size of such particles influence their interaction with the electric field.

The shape parameters of the bowl and dumbbell, d/σ (the ratio of the maximum thickness of the bowl and its diameter) and L/σ (the ratio of the center-to-center distance of the composing spheres and their diameter), respectively, as well as their theoretical construction, are given in Fig. 3. For the bowl, $d/\sigma = 0$ is the limit of an infinitesimally thin hemispherical shell, $d/\sigma = 1/2$ corresponds to a half sphere, and $d/\sigma = 1$ corresponds to a sphere. For the dumbbell, $L/\sigma = 0$ refers to a sphere, $L/\sigma = 1$ corresponds to two touching spheres, and

for $L/\sigma > 1$, the spheres are actually separated by a gap. The locations of the atoms in the clusters can be inferred by intersecting the cluster shape with a lattice of our choice. In the present work, we will focus on a simple cubic lattice.⁵² Examples of resulting clusters are depicted in Fig. 4, in which our choice of coordinate system is also defined, such that the cluster polarizabilities are diagonal with $\alpha_{xx} = \alpha_{yy}$.

A. Bowls

In Fig. 5(a), we plot α_{xx} and α_{zz} for a bowl-shaped particle, consisting of atoms on a sc lattice with lattice spacing

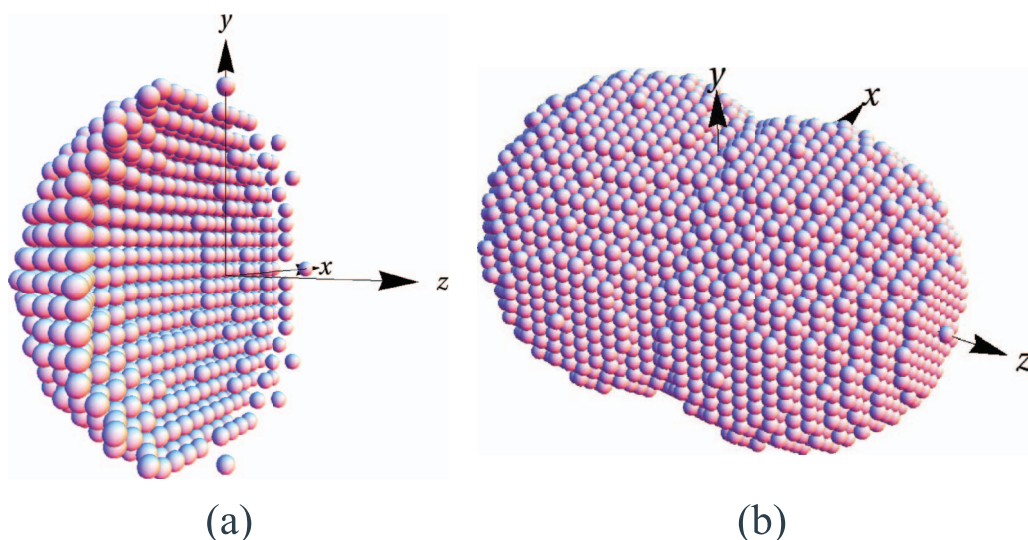


FIG. 4. Examples of the dipole setup for (a) a bowl (shape parameter $d/\sigma = 0.275$) and (b) a dumbbell (shape parameter $L/\sigma = 0.55$), both intersected with a simple cubic lattice. Each sphere corresponds to an inducible dipole (Lorentz atom).

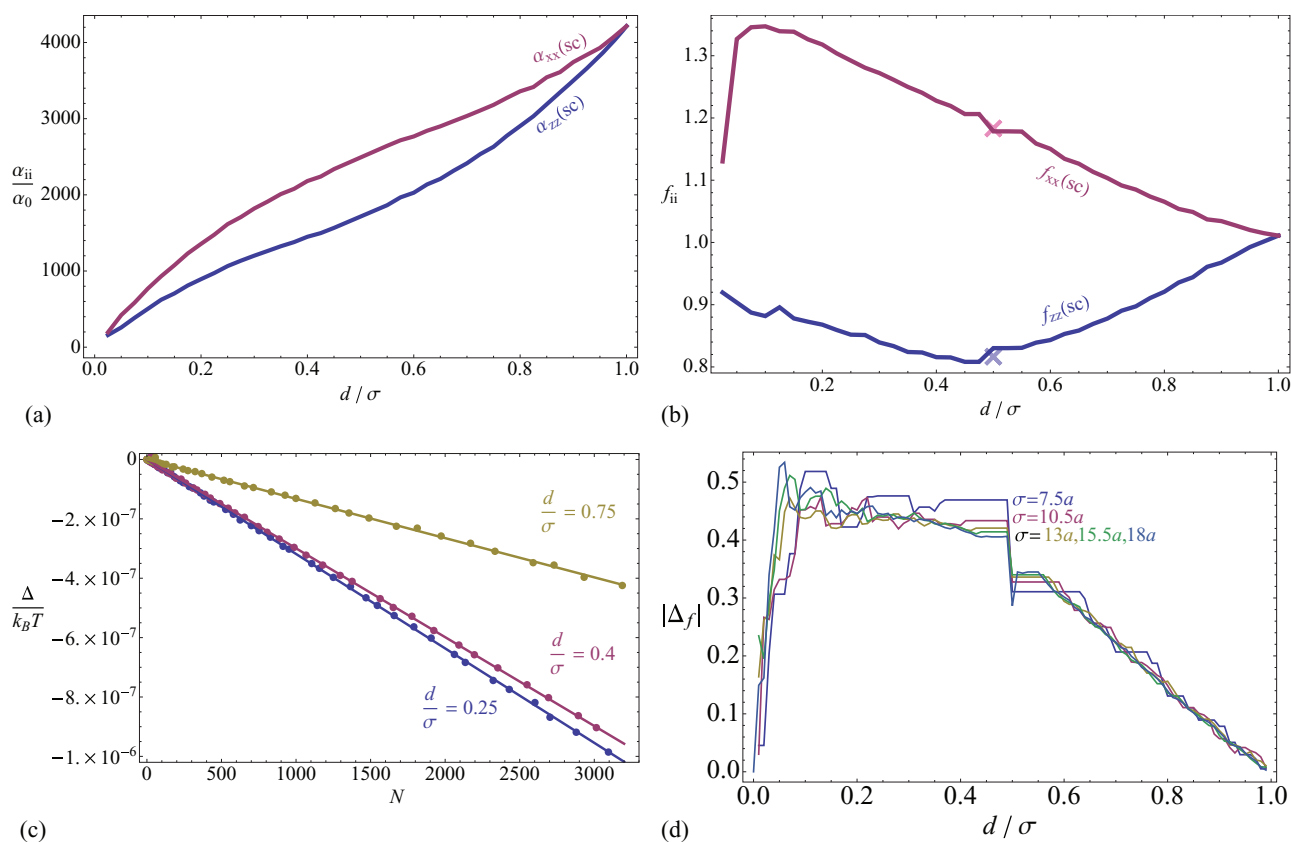


FIG. 5. Quantities associated with a bowl-shaped cluster of atoms on a simple cubic (sc) lattice with dimensionless lattice constant $\tilde{a} = 2$, shape parameter d/σ , and diameter σ [illustrated in Fig. 3(a)]. For $\sigma/a = 20$, panel (a) shows the elements α_{xx} (red) and α_{zz} (blue) of the polarizability tensor, and (b) the elements f_{xx} (red) and f_{zz} (blue) of the enhancement factor tensor, both as a function of d/σ . The light red and blue crosses in panel (b) indicate the enhancement factor elements of a hemisphere as calculated using continuum theory in Ref. 33. Panel (c) shows the energy difference of turning a bowl from its least to its most favorable orientation in an external electric field $E_0 = 100 \text{ V mm}^{-1}$, as a function of the number of atoms in the bowl, for $d/\sigma = 0.25, 0.4$, and 0.75 . The atomic polarizability is 5.25 \AA^3 (yielding lattice constant $a \approx 3.48 \text{ \AA}$) and the temperature is $T = 293 \text{ K}$. Panel (d) shows the difference $|\Delta_f| = |f_{zz} - f_{xx}|$ of the enhancement factor elements in the z and x directions, as a function of d/σ , for $\sigma/a = 7.5, 10.5, 13, 15.5$, and 18 , showing a strong dependence on the shape parameter d/σ and a weak dependence on the size parameter σ/a .

$\tilde{a} = 2$ and fixed bowl diameter $\sigma/a = 20$, as a function of the shape parameter d/σ , defined in Fig. 3. As expected, both α_{xx} and α_{zz} rise as d/σ increases from $d/\sigma = 0$ (a hemispherical shell) to $d/\sigma = 1$ (a sphere), because the number of atoms increases. Clearly, however, $\alpha_{xx} > \alpha_{zz}$ for all d/σ except $d/\sigma = 1$, meaning that the bowl is more polarizable in the x direction and, hence, from Eq. (12), has a lower orientational energy when the field is along the x direction.

Plotting the diagonal elements of the enhancement factor matrix in Fig. 5(b), we note that f_{xx} increases upon decreasing d , but that f_{zz} reaches a minimum at around $d/\sigma \approx 0.5$, where the interactions' diminishing effect on the polarizability in the z direction is largest. In the same figure, we indicate the results for a hemisphere (corresponding to $d/\sigma = 0.5$), as presented in Ref. 33. Considering that the theoretical approach presented in that work is completely different from ours, the agreement is excellent.

The orientational energy difference Δ for bowls composed of atoms on a sc lattice is plotted in Fig. 5(c) as a function of the number of atoms N for several values for d/σ , for an electric field strength $E_0 = 100 \text{ V mm}^{-1}$, an atomic polarizability $\alpha_0 = 5.25 \text{ \AA}^3$, and at room temperature ($T = 293 \text{ K}$). To the numerical results, linear functions

of form (20) have been fitted to determine Δ_f , which we now find to be negative. This implies that the axis of rotational symmetry is, for bowl-shaped particles, the least favorable direction for the external field. The numerical data show that the individual values of f_{xx} and f_{zz} vary (slightly) with cluster size but that the difference Δ_f is essentially constant. The latter is illustrated in Fig. 5(d) where we plot $|\Delta_f|$ as a function of the shape parameter d/σ , for several different bowl diameters σ . These graphs clearly overlap for higher values of σ or d/σ , which means that for those values, Δ_f is indeed independent of the particle size parameter σ .

As an example, for $d/\sigma = 0.25$, we have as fit parameter $\Delta_f \approx -0.442$, which we can use to predict the size of a nanocluster for which the orientational energy difference $|\Delta| = k_B T$; using Eq. (21) with $E_0 = 100 \text{ V mm}^{-1}$ and $\alpha_0 = 5.25 \text{ \AA}^3$ yields $N^* \approx 3.1 \times 10^9$. Extrapolating from the phenomenological dependence of N on σ ($N \propto \sigma^3$), we expect to reach this number of particles for $\sigma^*/a \approx 2.7 \times 10^3$ (as a comparison, the presently shown data goes up to $\sigma/a = 37$). Since $a = 2\alpha_0^{1/3} \approx 3.5 \text{ \AA}$ in this case, we can estimate the diameter $\sigma^* \approx 1.0 \mu\text{m}$ beyond which the electric field becomes capable of aligning the bowls.

B. Dumbbells

In Fig. 6(a), we plot α_{xx} and α_{zz} for a dumbbell particle with fixed sphere diameter $\sigma/a = 20$, consisting of atoms on a sc lattice with spacing $\tilde{a} = 2$, as a function of the shape parameter L/σ , defined in Fig. 3. With increasing L/σ (and thus increasing L , since σ is fixed), the number of atoms increases, resulting in a rising trend of α_{ii} for $L/\sigma < 1$. For $L/\sigma > 1$ (two separate spheres), an increase in L no longer increases the number of particles and instead only increases the distance between particles in both spheres, reducing their interactions. The result is that α_{zz} decreases, while α_{xx} , which benefits from less interactions, keeps increasing. We note here that α_{zz} already starts decreasing *before* $L/\sigma = 1$, which can be explained by the fact that close to $L/\sigma = 1$, the number of particles does not increase enough with increasing L to make up for the larger distance between particles in different spheres.

We plot the enhancement factor elements f_{xx} and f_{zz} in Fig. 6(b). We notice here again that f_{zz} already “stalls” at $L/\sigma \approx 0.7$ and decreases before L/σ reaches unity, while f_{xx} displays the opposite behavior. Also note that, for $L > \sigma$, as the distance between the separate spheres increases, the enhancement factors decay to that of a single sphere.

This was to be expected as the enhancement factor of two spheres at infinite separation is equal to that of a single sphere. Again, we indicate in the graph results that are calculated in Ref. 34 using continuum theory for two touching spheres ($L/\sigma = 1$) and note the excellent agreement with our work.

The energy difference between the most and least favorable orientations is given by Eq. (19) and is plotted in Fig. 6(c) as a function of N for three different values of L/σ , for $E_0 = 100 \text{ V mm}^{-1}$, $\alpha_0 = 5.25 \text{ \AA}^3$, $\tilde{a} = 2$, and room temperature $T = 293 \text{ K}$. Using Eq. (20), the fit parameter for dumbbells with $L/\sigma = 0.85$ turns out to be $\Delta_f \approx 0.323$, such that the number of particles for which the energy difference becomes comparable to the thermal energy is $N^* \approx 4.3 \times 10^9$. This corresponds to $\sigma^*/a \approx 1.6 \times 10^3$, whereas the presently shown data goes up till $\sigma/a = 20.5$. Inserting $a \approx 3.5 \text{ \AA}$, we obtain $\sigma^* \approx 0.6 \mu\text{m}$ as an estimate for the typical dumbbell diameter for which the orientational energy becomes important.

In Fig. 6(d), we plot Δ_f as a function of the dumbbell shape parameter L/σ , for several size parameters σ . Clearly, since the graphs overlap, also for dumbbells, Δ_f is largely independent of the overall size, and depends only on the shape.

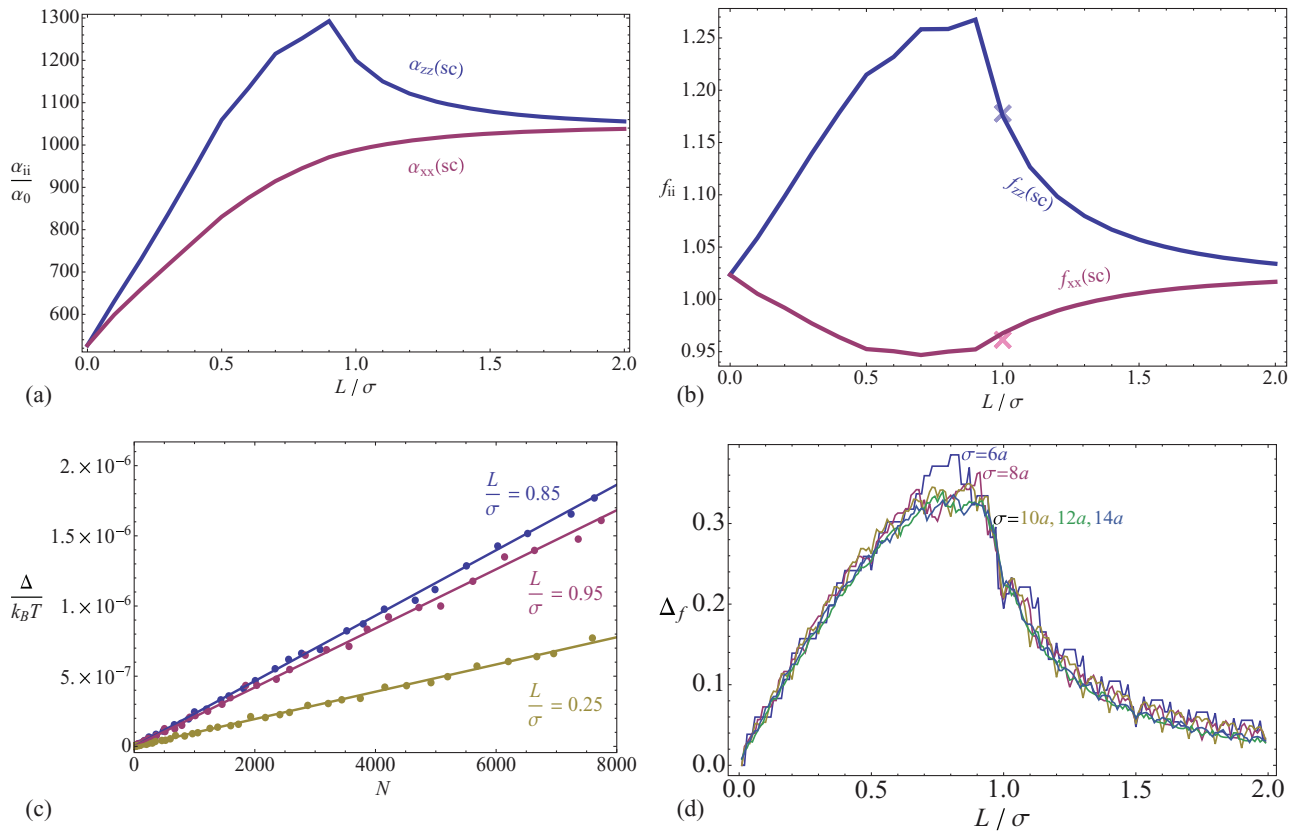


FIG. 6. Quantities associated with a dumbbell-shaped cluster of atoms on an simple cubic (sc) lattice with dimensionless lattice constant $\tilde{a} = 2$, with shape parameter L/σ , and dumbbell sphere diameter σ [illustrated in Fig. 3(b)]. For $\sigma/a = 20$, panel (a) shows the elements α_{xx} (red) and α_{zz} (blue) of the polarizability matrix and (b) the elements f_{xx} (red) and f_{zz} (blue) of the enhancement factor matrix as a function of L/σ . The light red and blue crosses in panel (b) indicate the enhancement factor elements of two touching spheres as calculated using continuum theory in Ref. 34. Panel (c) shows the energy difference of turning the dumbbell from its least to its most favorable orientation in an external electric field $E_0 = 100 \text{ V mm}^{-1}$, as a function of the number of atoms in the dumbbell, for $L/\sigma = 0.25, 0.85$, and 0.95 . The atomic polarizability is 5.25 \AA^3 (yielding lattice constant $a \approx 3.48 \text{ \AA}$) and the temperature is $T = 293 \text{ K}$. Panel (d) shows the difference $\Delta_f = f_{zz} - f_{xx}$ of the enhancement factor elements in the z - and x directions, as a function of L/σ , for $\sigma/a = 6, 8, 10, 12$, and 14 , again showing a strong shape- and a weak size-dependence.

V. THE ENHANCEMENT FACTOR OF DIELECTRIC CUBES

In the nonretarded limit of present interest, the interaction energy between dipoles separated by a distance r is $\propto r^{-3}$. In three dimensions, this is a long-range interaction which does not decay sufficiently quickly to ignore system size and boundary effects. Therefore, we should not expect to be able to determine bulk quantities from calculations such as those done in this paper. The enhancement factor difference Δ_f (discussed in Secs. III and IV), which is found to be essentially independent of size, seems to be an interesting exception.

In Ref. 26, the enhancement factor of one-dimensional lines and two-dimensional squares of atoms was determined and investigated in detail. For these low-dimensional systems the r^{-3} interaction is short-ranged, such that well-defined bulk behavior is found in the “middle” of these clusters, independent of the boundary layers. In this section, we aim to do the same for a cubic-shaped particle with atoms on a cubic lattice. We will confirm that the polarizability does not seem to reach a bulk value for this three-dimensional object. Interestingly, since the fully retarded interaction energy decays asymptotically as $\propto r^{-4}$, we may thus note that the existence of a well-defined polarizability (and hence permittivity) for real-life bulk substances can be qualified as a retardation effect: the fact the speed of light is finite results in substances having well-defined bulk permittivities.

A. Theoretical predictions

In Ref. 26, the (scalar) enhancement factor for a cubic $L \times L \times L$ cluster of atoms on a cubic lattice is plotted as a function of the rib length L . The enhancement factor is seen to increase with increasing cube size, seemingly approaching some limiting value greater than unity. In contrast, when it is assumed that all dipoles have the same polarization, it is possible to prove that^{26,45} $f(\infty \times \infty \times \infty) = 1$. However, by assuming the same polarization for all dipoles, we neglect the effect of the surfaces of the cube, which is questionable given the long range of the dipole-dipole potential ($\propto r^{-3}$). One might argue that an infinite lattice of atoms without any surface is the best model for a bulk substance imaginable, but realistic substances are never infinite and, as will be shown, their surfaces do have a significant effect on the polarizability even when their proportional number of atoms becomes low.

In Ref. 26 the enhancement factor is plotted for cube sizes up to $10 \times 10 \times 10$. This is still far from the regime where the surface can be expected to be negligible; the ratio of dipoles at the surface is, for this cube size, still $(10^3 - 8^3)/10^3 \approx 0.49$. In the present work, we will therefore consider larger cubic clusters, of sizes up to $120 \times 120 \times 120$. For these clusters, the fraction of surface dipoles is ~ 0.05 . Another prediction for the limiting value of $f(L \rightarrow \infty)$ can be obtained from the Clausius-Mosotti relation. For our purposes, a convenient form of this relation is given by⁵³

$$\mathbf{p}_c = \frac{N\alpha_0\mathbf{E}_0}{1 - n\alpha_0/3},$$

where n is the number density of atoms. For a simple cubic lattice, where the number density equals $n = 1/a^3$, the enhancement factor is thus given by

$$\mathbf{f} = \frac{1}{1 - \alpha_0/3a^3}\mathbf{I}. \quad (25)$$

The Clausius-Mosotti relation is expected to give a better prediction for lower densities.⁴⁵ Below, we will compare the prediction of Eq. (25) to numerical results as a function of the dimensionless lattice constant $\tilde{a} = a/\alpha_0^{1/3}$.

B. Numerical methods

Special optimization techniques were used in the case of large dielectric cubes. Because the number of atoms in the cluster increases rapidly with the rib length of the cube, we encounter practical problems such as memory limitations. However, two techniques can be used to reduce this problem, which we will now briefly discuss.

1. Exploiting symmetry

In this technique, we use the symmetries of the cube to reduce the order of the linear equation to be solved. It is possible to express the polarizations of all the dipoles in terms of only those in one octant of the cube. If we insert these relations into the set of Eqs. (11), we reduce the number of dipoles by a factor of 8. Note that in this way, we also increase the computational cost of calculating a matrix element by (roughly) a factor of 8, but since the cost of solving a set of linear equations scales with the square of the order of the equation set, we gain an overall factor of 8 in computation speed.

2. The Gauss-Seidel method

The second technique uses the Gauss-Seidel method⁵⁴ for solving a set of linear equations, trading computation speed for less memory use. The Gauss-Seidel method is an iterative method for solving \mathcal{P} from an equation of form (11). The method starts with a guess (discussed below) for \mathcal{P} , which we shall call $\mathcal{P}^{(0)}$. The next approximation for \mathcal{P} , $\mathcal{P}^{(1)}$, is calculated using the following formula:

$$p_i^{(k+1)} = \frac{1}{z_{ii}} \left(e_i - \sum_{j>i} z_{ij} p_j^{(k)} - \sum_{i>j} z_{ij} p_j^{(k+1)} \right), \quad (26)$$

where the $p_i^{(k)}$ are the elements of $\mathcal{P}^{(k)}$, the e_i are the elements of \mathcal{E} , and the z_{ij} are the elements of the matrix $(\mathcal{I} - \alpha_0\mathcal{T})$. Note that in our case $z_{ii} = 1$, and that we can write Eq. (26) in terms of more familiar quantities,⁵¹

$$\mathbf{p}_i^{(k+1)} = \mathbf{E}_0 - \sum_{j>i} \mathbf{Z}_{ij} \cdot \mathbf{p}_j^{(k)} - \sum_{i>j} \mathbf{Z}_{ij} \cdot \mathbf{p}_j^{(k+1)},$$

where the \mathbf{Z}_{ij} are 3×3 blocks in the matrix $(\mathcal{I} - \alpha_0\mathcal{T})$. Note that with this technique, it is not necessary to store a “new” and an “old” copy of \mathcal{P} , because only elements are needed that have been calculated previously; i.e., it is no problem to simply keep overwriting the elements of \mathcal{P} .

TABLE II. An overview of techniques used for calculating the polarizability of a cubic cluster of atoms on a simple cubic lattice, and their associated acronyms, as used in the caption of Fig. 7. In the LAPACK methods, we load the elements of the matrix in memory to the numerical precision specified in the “Precision” column and use the routines in the LAPACK package to solve the relevant set of linear equations. The Gauss-Seidel methods involve (re-)calculating the elements of the matrix on the fly and, starting from an initial guess, using 20 iterations of the Gauss-Seidel method to solve the set of linear equations. The “Symmetries” column refers to whether or not the symmetries of the dielectric cube were exploited. The “ L_{max} ” column lists estimates for largest feasible rib lengths that each method can handle, given our available resources.

Acronym	Method	Symmetries	Precision	L_{max}
NDL	LAPACK	No	Double	20
SDL	LAPACK	Yes	Double	40
SSL	LAPACK	Yes	Single	48
NGS	Gauss-Seidel	No	Double	60
SGS	Gauss-Seidel	Yes	Double	120

As an initial guess we construct $\mathcal{P}^{(0)}$ as follows: we sum the \mathbf{Z}_{ij} horizontally and then solve the equation

$$\left(\sum_{j=1}^N \mathbf{Z}_{ij} \right) \cdot \mathbf{p}_i^{(0)} = \mathbf{E}_0$$

for each $\mathbf{p}_i^{(0)}$. Using this guess, the enhancement factor could be calculated to a precision of 10 digits within 20 iterations.

Since \mathbf{Z}_{ij} can be (re-)calculated on the fly as needed and the elements of \mathcal{E} can be inferred using only a three-dimensional vector, we only need to store $\sim 3N$ numbers, i.e., the elements of \mathcal{P} . This effectively eliminates the memory problem. However, as a consequence, the resulting calculation is much slower than the one that uses the LAPACK routine.

By combining the two techniques (symmetry exploitation and the Gauss-Seidel method), we were able to calculate the enhancement factor for cubes as large as $120 \times 120 \times 120$. The data points presented in Subsection V C have been calculated using various methods, corresponding to combinations of applying the two aforementioned techniques. In Table II, we give an overview of these methods, and define the acronyms that are used in the caption of Fig. 7.

The different methods have all been tested for consistency and the agreement between them is excellent. Computationally, the most practical techniques were the SDL-method for small rib lengths, because of its speed and simple implementation, and the SGS-method for large rib lengths, because of its negligible memory usage.

C. Numerical results

In Fig. 7(a), the (scalar) enhancement factor f of $L \times L \times L$ cubes, as calculated numerically, is plotted as a function of L , for several (dimensionless) lattice spacings \tilde{a} . For all of the lattice spacings, the qualitative behavior of the enhancement factor is the same: for low L , it increases rapidly as a function of L , but starts to level off at $L \approx 10$, seemingly reaching a limiting value $f(L) > 1$ around $L \approx 20$. This agrees reasonably well with prediction (25) made using the Clausius-Mossotti relation, and contradicts the pre-

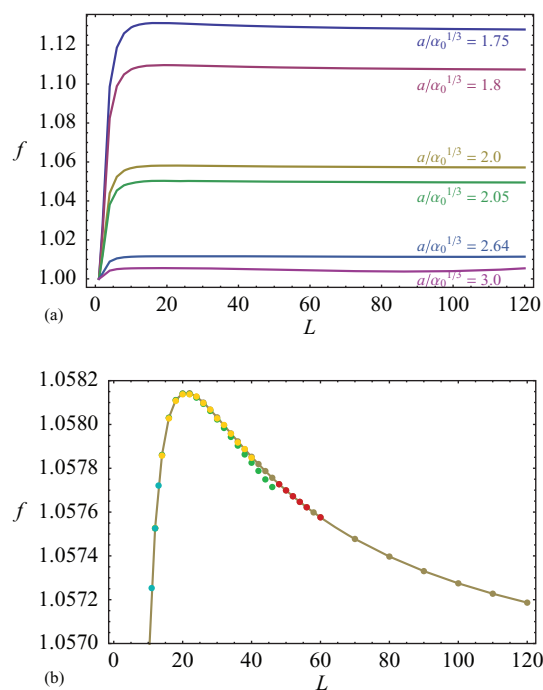


FIG. 7. The enhancement factor f of a cubic $L \times L \times L$ cluster with atoms on a cubic lattice, as a function of the number of atoms along the rib L , in (a) for the dimensionless lattice spacings $\tilde{a} = 1.75$ (blue), $\tilde{a} = 1.8$ (red), $\tilde{a} = 2.0$ (yellow), $\tilde{a} = 2.05$ (green), $\tilde{a} = 2.64$ (light blue), and $\tilde{a} = 3.0$ (purple), and in (b) a zoom-in (along the vertical axis) for $\tilde{a} = 2.0$ with the data points generated by different numerical methods (see text and Table II): SGS (dark yellow points and curve), NGS (red points), SSL (green points), SDL (bright yellow points), and NDL (light blue points). Note that SSL slightly underestimates f for $L \approx 40$.

diction $f(\infty) = 1$ (made by ignoring the edges of the cube). We investigate the behavior with a particular lattice spacing, $\tilde{a} = 2$, in full detail. Figure 7(b) shows a (vertical) zoom-in of Fig. 7(a), including data points as generated by various numerical methods. It can be seen from Fig. 7(b) that the enhancement factor (for $\tilde{a} = 2$) reaches a maximum value of $f \approx 1.05814$ at $L = 20$, after which it starts decreasing, where the rate of decrease reaches a maximum at $L = 34$. This behavior is the same for all other values of \tilde{a} , albeit with different values of f .

The decrease of f observed beyond $L = 34$ is so slow that it could, conceivably, be caused by systematic rounding errors in the calculation of the elements of the matrix. This is still an open question that may be approached in a number of different ways, for example, by increasing the cube size and observing whether the enhancement factor keeps decreasing; another approach might be to increase the precision to which the elements of the matrix are calculated and observe whether this affects the value of the enhancement factor. A relevant observation here is that the single precision method SSL gives slightly lower results (for large L) than the double precision methods. However, the difference does not appear to be large enough to expect the decline to vanish for asymptotically large precisions.

It is clear that we have not been able to determine a limiting value for f . The decay observed beyond $L = 34$ slows down as L increases, but a reliable extrapolation to

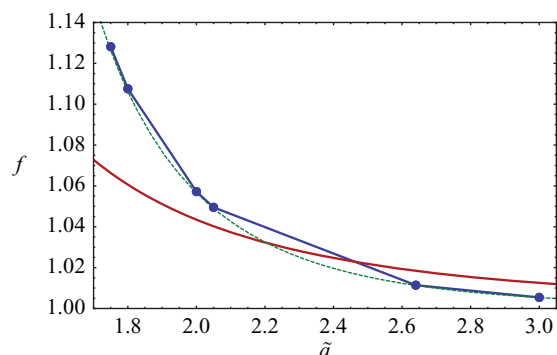


FIG. 8. The enhancement factor f of a $120 \times 120 \times 120$ cube of atoms, as a function of the (dimensionless) lattice constant $\tilde{a} = a/\alpha_0^{1/3}$. In blue, the numerical results are plotted, while in red, the prediction as given by the Clausius-Mosotti relation, Eq. (25), is shown. The dashed green line is Eq. (22) of Ref. 32, where the enhancement factor is calculated using continuum theory. Note the excellent agreement between the latter and our result, despite the completely different approaches.

asymptotically large cubes could not be determined. Therefore, bulk behavior was not reached for our cube sizes. We stress again that this conclusion was reached *not* based on the absolute value of f at $L = 120$, but based on the variation that we observe for large L .

In Fig. 8, we plot the enhancement factor of a $120 \times 120 \times 120$ cube as a function of its dimensionless lattice constant \tilde{a} , together with the Clausius-Mosotti prediction of Eq. (25). As expected, the Clausius-Mosotti prediction is better for larger lattice constants (i.e., lower densities). Note that with increasing \tilde{a} , Eq. (25) changes from an under- to an over-estimation of the enhancement factor. In the same figure, we plot the results as presented in Eq. (22) of Ref. 32. We note the excellent agreement, despite the fact that the two results are calculated in completely different ways.

1. Local enhancement factor

Apart from the global enhancement factor f discussed until now, it is also of interest to consider its local counterpart in finite clusters. Choosing the z direction to lie along the external electric field \mathbf{E}_0 [see Fig. 9(a)], we define the local enhancement factor f' as the z -component of the polarization of the local atom, divided by $\alpha_0 E_0$. Note that, using this definition, the analogy with the global enhancement factor f is not complete, because even when the electric field is applied in the z direction, the polarization of the individual atoms can have nonzero components in the x and y directions. Consequently, if we were to express the local polarization as

$$\mathbf{p} = \mathbf{f}' \cdot \alpha_0 \mathbf{E}_0,$$

where \mathbf{f}' would be a 3×3 matrix, then \mathbf{f}' would not be diagonal.

In Figs. 9(b) and 9(c), we plot the local enhancement factor f' along two planes cut through the middle of a $120 \times 120 \times 120$ cube, as illustrated in Fig. 9(a). From the shape of the graph we clearly see that f' is not a spatial constant and varies most pronouncedly on the faces and in the corners of the cube. In Fig. 9(b) we observe that the sides of the cube normal to the electric field ($z = \pm 60a$) experi-

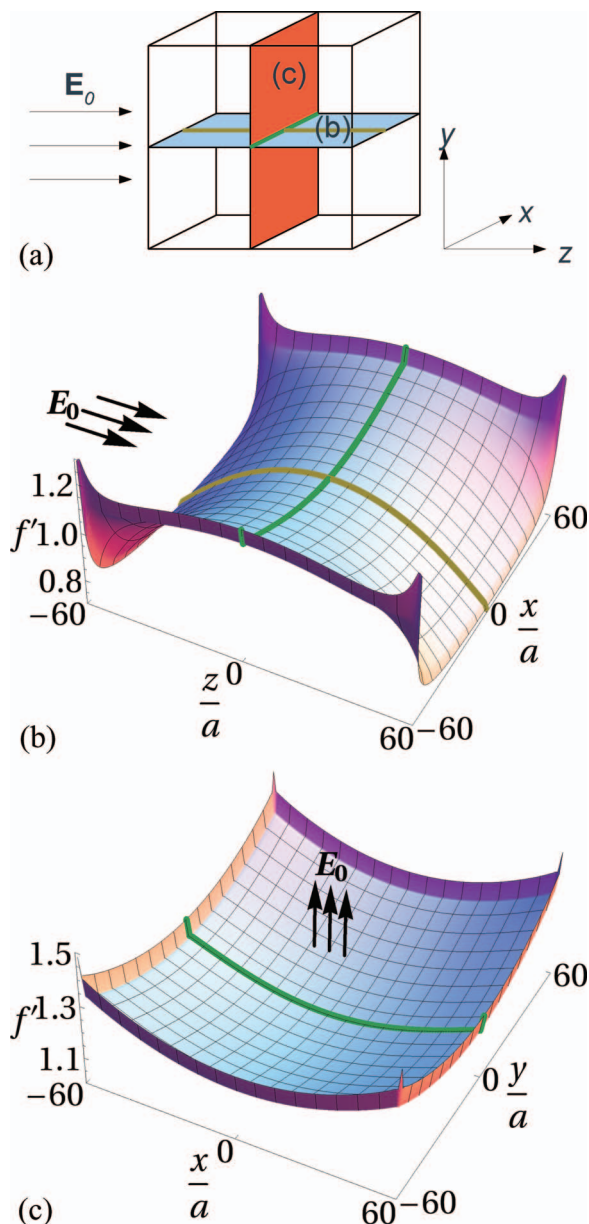


FIG. 9. (a) The orientation of the planes, cube, electric field, and coordinate system with respect to each other: the planes are cut through the middle of the cube, in the x - z plane and the x - y plane, while the electric field is applied in the z direction. The cube is oriented such that the ribs lie along the Cartesian directions. The (green) line along the x axis denotes the intersection of the two planes and is also represented in panels (b) and (c). (b) and (c) The local enhancement factor f' (defined in the text) of two sheets of dipoles lying on perpendicular planes, cut through the middle of a $120 \times 120 \times 120$ cube of dipoles on a cubic lattice, with lattice constant $\tilde{a} = 2$. Panel (b) corresponds to the blue and panel (c) corresponds to the red plane as depicted in panel (a). The yellow and green lines appearing in this figure also correspond to the directions along which we plot the local enhancement factor in Fig. 10.

ence a clear polarization reduction (i.e., $f' < 1$), e.g., reaching a local enhancement factor of $f' \approx 0.71335$ in the middle of the face (at $x = 0$, $y = 0$, and $z = \pm 60a$). The interior of the cube turns out to experience a slight enhancement of $f' \approx 1.04530$ in the center $x = y = z = 0$ (not visible from the graphs). A more dramatic enhancement is experienced by the faces of the cube that lie in-plane with the electric field (e.g., $x = \pm 60a$); for example, at $z = 0$, the enhancement on

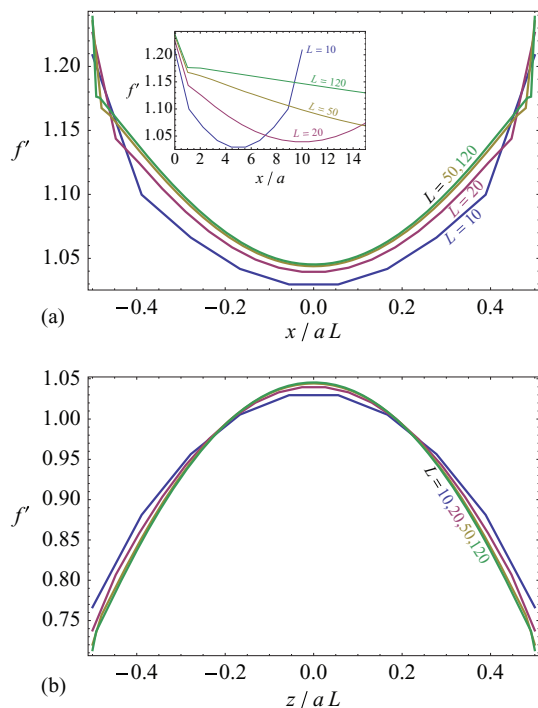


FIG. 10. The local enhancement factor f' along a straight line in (a) the x direction ($\perp E_0$, illustrated in green in Fig. 9) and (b) the z direction ($\parallel E_0$, illustrated in yellow in Fig. 9), through the middle of a cubic cluster of atoms on a simple cubic lattice with lattice spacing $\tilde{a} = 2$, for cube rib lengths $L = 10, 20, 50$, and 120 . In both panels, the rib length was scaled out, but in the inset of panel (a), we also plot f' as a function of the absolute x -coordinate.

the faces is $f' \approx 1.23876$, while in the corner ($z = \pm 60a$), $f' \approx 1.29005$, as mentioned earlier.

In Fig. 10, we plot the local enhancement factor along a line parallel and one perpendicular to the electric field, both through the middle of the cube (these lines are also illustrated in Fig. 9), for several values of L , as a function of scaled coordinates. The behavior of the local enhancement factor, as seen in Figs. 9 and 10, shares many features also seen in the case of two-dimensional squares, as discussed in Ref. 26: we observe high local enhancement on all edges of planes perpendicular to the electric field, high local enhancement on the edges parallel to the electric field of planes in-plane with the electric field, and low local enhancement on the edges perpendicular to the electric field of planes in-plane with the electric field. Furthermore, the local enhancement varies by far the most rapidly at locations close to the edge. Like in Ref. 26, for all values of L the outer layer of atoms in faces parallel to the electric field is especially polarized. This is illustrated in the inset of Fig. 10(a), but is also visible in Fig. 9. In this layer of atoms, the local enhancement factor appears to depend more strongly on L and a limiting value for the on-edge local enhancement was not reached for the cube sizes considered in the present work (up to $L = 120$). Whether such a limiting value exists for the edge is therefore unclear at this point.

An important difference with two-dimensional squares is that the local enhancement factor in a cube varies significantly in the interior of the cube (albeit less than on the edge). Focusing now on Fig. 10, we observe that, upon varying L , the local

enhancement factor in the interior of the cube, as a function of scaled coordinates, goes to a limiting behavior for large L . This means that the (absolute) “penetration depth” of the electric field into the cluster is *not*, as in Ref. 26, independent of the cluster size, but is instead approximately proportional to L .

An analysis of the “polarization charge” density $\nabla \cdot \mathbf{P}$ (where \mathbf{P} stands for the local polarization density) shows that it is nonzero (albeit small) for the cube sizes achieved here, but that its magnitude is inversely proportional to the cube rib length. In the limit of infinitely large cubes, we thus expect to reach $\nabla \cdot \mathbf{P} = 0$, as required by continuum theory. Indeed, already for a $120 \times 120 \times 120$ cube, most of the variation of the local enhancement can safely be ascribed to the electric field varying inside the cube like that seen in continuum theory. However, this does not change the fact that the interior of the cube does not behave like a bulk substance, since in bulk one expects the system to be translation invariant, with no surface effects. The reason that in our system the edges remain important even as the cube is scaled is the long range of the dipole-dipole interaction ($\propto r^{-3}$). If we were to include retardation effects, the dipole-dipole interaction would scale (for large r) as $\propto r^{-4}$, and upon scaling the cube, the interior *would* become a bulk substance, with surface effects vanishing as the cube size is taken to infinity. Thus, the very existence of bulk dielectric substances in nature may be seen as a retardation effect.

VI. CONCLUSIONS AND OUTLOOK

The CDM is a rigorous tool to include many-body interatomic interactions on the basis of a polarizable atom model, not only in the potential energy but also in other quantities such as the polarizability of a cluster of atoms. The applicability of the method is limited by computing power and becomes unfeasible for atom numbers larger than $\mathcal{O}(10^4)$. This corresponds to very small nanoparticles, slightly below the experimentally realizable regime. However, as has been shown in this article, it is in most cases fairly straightforward to extrapolate some of the key properties to larger cluster sizes.

We have discussed the polarizability and orientational energy of cuboids, bowls, dumbbells, and cubes. In general, these clusters are all most polarizable in the direction of their largest dimension: for cuboids along their longest rib, for bowls in the directions perpendicular to their axis of rotational symmetry, and for dumbbells along their rotational symmetry axis. These directions are also the preferred orientations of the cluster in an external electric field. Cubes are equally polarizable in all directions, and thus have no preferred orientation in an external electric field.

We then turned our attention to the magnitude of the energy difference Δ between the most- and least-favored orientations of each cluster shape. We found that, for typical experimental values for electric field strength, temperature, and atomic polarizability, these energy differences are small compared to the thermal energy (for the atom numbers that are feasible with our computer resources). However, we also found an almost exact linear dependence of Δ on the number of cluster atoms N , and related the slope of the graph to

the difference Δ_f in enhancement factor diagonal elements, a quantity that turns out to be independent of the cluster size and that depends only on the cluster shape and lattice spacing. The dependence of Δ_f on the cluster shape was then investigated. This was done for several cluster sizes in order to prove the size-independence of Δ_f . Using the linear dependence of Δ on N , we estimated, for some chosen cluster shapes, the number of atoms (and hence the spatial dimensions of the cluster) for Δ to be of the order of the thermal energy. This is relevant because it gives an estimate for when a dielectric colloid might be aligned in an external electric field. The estimates, for some typical experimental parameters, all have values of roughly $1 \mu\text{m}$ for the longest dimension of the colloid. In other words, dielectric nanoparticles are not easily aligned by external electric fields.

The enhancement factor of a cubic cluster of atoms on a simple cubic lattice at first glance seems to go to a well-defined asymptotic value. However, closer inspection reveals that, in fact, the enhancement factor starts decreasing again as the rib length increases and whether a limiting value of the enhancement factor exists is still unclear at this point. As shown, the local enhancement factor does not reach a plateau in the interior of the cube, even for the largest cubes, and so the question of whether bulk behavior will be reached, judging from the results presented here, seems to have “no” as an answer. This can be attributed to the long range ($\propto r^{-3}$) character of the dipole-dipole interaction, and hence retardation (which results in an interaction $\propto r^{-4}$) may be seen as the cause of the well-defined bulk dielectric properties as observed in nature.

ACKNOWLEDGMENTS

This work is part of the research programme of FOM, which is financially supported by NWO. Financial support by an NWO-VICI grant is acknowledged.

- ¹S. C. Glotzer and M. J. Solomon, *Nature Mater.* **6**, 557 (2007).
- ²S.-M. Yang, S.-H. Kim, J.-M. Lim, and G.-R. Yi, *J. Mater. Chem.* **18**, 2177 (2008).
- ³M. Grzelczak, J. Vermant, E. M. Furst, and L. M. Liz-Marzán, *ACS Nano* **4**, 3591 (2010).
- ⁴M. J. Solomon, *Curr. Opin. Colloid Interface Sci.* **16**, 158 (2011).
- ⁵S. C. Glotzer, M. A. Horsch, C. R. Iacovella, Z. Zhang, E. R. Chan, and X. Zhang, *Curr. Opin. Colloid Interface Sci.* **10**, 287 (2005).
- ⁶B. Nikoobakht, Z. L. Wang, and M. A. El-Sayed, *J. Phys. Chem. B* **104**, 8635 (2000).
- ⁷D. Fava, Z. Nie, M. A. Winnik, and E. Kumacheva, *Adv. Mater.* **20**, 4318 (2008).
- ⁸E. L. Thomas, *Science* **286**, 1307 (1999).
- ⁹D. J. Kraft, W. S. Vlug, C. M. van Kats, A. van Blaaderen, A. Imhof, and W. K. Kegels, *J. Am. Chem. Soc.* **131**, 1182 (2009).
- ¹⁰I. D. Hosein, S. H. Lee, and C. M. Liddell, *Adv. Funct. Mater.* **20**, 3085 (2010).
- ¹¹L. Onsager, *Ann. N.Y. Acad. Sci.* **51**, 627 (1949).
- ¹²K. M. Ryan, A. Mastroianni, K. A. Stancil, H. T. Liu, and A. P. Alivisatos, *Nano Lett.* **6**, 1479 (2006).
- ¹³D. van der Beek, A. V. Petukhov, P. Davidson, J. Ferré, J. P. Jamet, H. H. Wensink, G. J. Vroege, W. Bras, and H. N. W. Lekkerkerker, *Phys. Rev. E* **73**, 041402 (2006).
- ¹⁴K. Bubke, H. Gnewuch, M. Hempstead, J. Hammer, and M. L. H. Green, *Appl. Phys. Lett.* **71**, 1906 (1997).
- ¹⁵A. F. Demirörs, P. M. Johnson, C. M. van Kats, A. van Blaaderen, and A. Imhof, *Langmuir* **26**, 14466 (2010).

- ¹⁶P. A. Smith, C. D. Nordquist, T. N. Jackson, T. S. Mayer, B. R. Martin, J. Mbindyo, and T. E. Mallouk, *Appl. Phys. Lett.* **77**, 1399 (2000).
- ¹⁷D. V. Talapin, E. V. Shevchenko, C. B. Murray, A. Kornowski, S. Forster, and H. Weller, *J. Am. Chem. Soc.* **126**, 12984 (2004).
- ¹⁸S. Ahmed and K. M. Ryan, *Nano Lett.* **7**, 2480 (2007).
- ¹⁹B. Q. Sun and H. Siringhaus, *J. Am. Chem. Soc.* **128**, 16231 (2006).
- ²⁰D. Nagao, C. M. van Kats, K. Hayasaka, M. Sugimoto, M. Konno, A. Imhof, and A. van Blaaderen, *Langmuir* **26**, 5208 (2010).
- ²¹M. Marechal, R. J. Kortschot, A. F. Demirörs, A. Imhof, and M. Dijkstra, *Nano Lett.* **10**, 1907 (2010).
- ²²I. D. Hosein and C. M. Liddell, *Langmuir* **23**, 8810 (2007).
- ²³L. Rossi, S. Sacanna, and K. P. Velikov, *Soft Matter* **7**, 64 (2011).
- ²⁴X. D. Wang, E. Graugnard, J. S. King, Z. L. Wang, and C. J. Summers, *Nano Lett.* **4**, 2223 (2004).
- ²⁵C. Zoldesi, C. A. van Walree, and A. Imhof, *Langmuir* **22**, 4343 (2006).
- ²⁶H.-Y. Kim, J. O. Sofo, D. Velegol, M. W. Cole, and G. Mukhopadhyay, *Phys. Rev. A* **72**, 053201 (2005).
- ²⁷M. W. Cole, D. Velegol, H.-Y. Kim, and A. A. Lucas, *Mol. Simul.* **35**, 849 (2009).
- ²⁸C. A. Utreras-Díaz, E. Martín García, and M. A. R. Troncoso, *Phys. Status Solidi B* **190**, 421 (1995).
- ²⁹M. Manninen, R. M. Nieminen, and M. J. Puska, *Phys. Rev. B* **33**, 4289 (1986).
- ³⁰W. D. Knight, K. Clemenger, W. A. de Heer, and W. A. Saunders, *Phys. Rev. B* **31**, R2539 (1985).
- ³¹A. Sihvola, *J. Nanomater.* **2007**, 45090 (2007).
- ³²A. Sihvola, P. Ylä-Oijala, S. Järvenpää, and J. Avelin, *IEEE Trans. Antennas Propag.* **52**, 2226 (2004).
- ³³H. Kettunen, H. Wallén, and A. Sihvola, *J. Appl. Phys.* **102**, 044105 (2007).
- ³⁴M. Pitkonen, *J. Appl. Phys.* **103**, 104910 (2008).
- ³⁵M. Pitkonen, *J. Math. Phys.* **47**, 102901 (2006).
- ³⁶M. J. Renne and B. R. A. Nijboer, *Chem. Phys. Lett.* **1**, 317 (1967).
- ³⁷B. R. A. Nijboer and M. J. Renne, *Chem. Phys. Lett.* **2**, 35 (1968).
- ³⁸M. W. Cole and D. Velegol, *Mol. Phys.* **106**, 1587 (2008).
- ³⁹F. London, *Z. Phys.* **63**, 245 (1930).
- ⁴⁰I. E. Dzyaloshinskii, E. M. Lifshitz, and L. P. Pitaevskii, *Adv. Phys.* **10**, 165 (1961).
- ⁴¹H. C. Hamaker, *Physica* **4**, 1058 (1937).
- ⁴²J. H. de Boer, *Trans. Faraday Soc.* **32**, 10 (1936).
- ⁴³B. Derjaguin and L. Landau, *Acta Physicochim. URSS* **14**, 633 (1941).
- ⁴⁴E. J. W. Verwey and J. T. G. Overbeek, *Theory of the Stability of Lyophobic Colloids* (Elsevier, New York, 1948).
- ⁴⁵J. D. Jackson, *Classical Electrodynamics*, 3rd ed. (Wiley, New York, 1999).
- ⁴⁶H.-Y. Kim, J. O. Sofo, D. Velegol, M. W. Cole, and A. A. Lucas, *J. Chem. Phys.* **124**, 074504 (2006).
- ⁴⁷S. M. Gatica, M. W. Cole, and D. Velegol, *Nano Lett.* **5**, 169 (2005).
- ⁴⁸H.-Y. Kim, J. O. Sofo, D. Velegol, M. W. Cole, and A. A. Lucas, *Langmuir* **23**, 1735 (2007).
- ⁴⁹This proof relies on the fact that $\mathbf{D}_{ij} = \mathbf{D}_{ij}^T$, which, in turn, can be proven by using induction in combination with the general expression for the inverse of a matrix built up of submatrices:

$$\begin{pmatrix} \mathbf{K} & \mathbf{L} \\ \mathbf{M} & \mathbf{N} \end{pmatrix}^{-1} = \begin{pmatrix} \mathbf{K}^{-1} + \mathbf{K}^{-1}\mathbf{L}\mathbf{S}^{-1}\mathbf{M}\mathbf{K}^{-1} & -\mathbf{K}^{-1}\mathbf{L}\mathbf{S}^{-1} \\ -\mathbf{S}^{-1}\mathbf{M}\mathbf{K}^{-1} & \mathbf{S}^{-1} \end{pmatrix},$$

where

$$\mathbf{S} = (\mathbf{N} - \mathbf{M}\mathbf{K}^{-1}\mathbf{L}).$$

- ⁵⁰See <http://www.netlib.org/lapack/> for information and downloadable versions of LAPACK.
- ⁵¹From Eq. (18), we could also have derived an explicit expression for the orientational energy of the cluster shapes discussed in this article:

$$\begin{aligned} V_E &= -\frac{1}{2}[(\mathbf{E}_0 \cdot \hat{x})^2 + (\mathbf{E}_0 \cdot \hat{y})^2]\alpha_{xx} - \frac{1}{2}(\mathbf{E}_0 \cdot \hat{z})^2\alpha_{zz} \\ &= -\frac{1}{2}(\alpha_{xx} + (\alpha_{zz} - \alpha_{xx})\cos^2\theta)E_0^2, \end{aligned}$$

where in the first line we used $\alpha_{xx} = \alpha_{yy}$ and in the second line, we introduced the angle θ between \mathbf{E}_0 and the z axis. From the resulting expression,

it is clear that the extrema of the orientational energy are located at $\theta = 0$ and $\theta = \pi/2$ and that the difference in orientational energy between the two extrema is indeed given by Eq. (19).

⁵²For bowls and dumbbells, calculations were also done using a face-centered cubic lattice. The results are qualitatively the same. Quantitatively, the enhancement factors tend to differ from unity more with an fcc lattice than with a sc lattice, which can be attributed to the higher density of atoms,

resulting in stronger atom-atom interactions and hence stronger many-body effects.

⁵³J. H. Hannay, *Eur. J. Phys.* **4**, 141 (1983).

⁵⁴R. Barrett, M. Berry, T. F. Chan, J. Demmel, J. Donato, J. Dongarra, V. Eijkhout, R. Pozo, C. Romine, and H. van der Vorst, *Templates for the Solution of Linear Systems: Building Blocks for Iterative Methods* (SIAM, Philadelphia, 1994).